Journal of Physics: Conference Series **2889** (2024) 012062 doi:10.1088/1742-6596/2889/1/012062

Time-dependent Aharonov-Bohm effect for electromagnetic and gravitational scalar potentials

RY Chiao
University of California, Merced, School of Natural Sciences, Merced, CA 95344, USA
E-mail: raymond_chiao@yahoo.com

NA Inan
Clovis Community College, 10309 N. Willow, Fresno, CA 93730 USA
University of California, Merced, School of Natural Sciences, Merced, CA 95344, USA
Department of Physics, California State University Fresno, Fresno, CA 93740-8031, USA
E-mail: ninan@ucmerced.edu

M Scheibner
University of California, Merced, School of Natural Sciences, Merced, CA 95344, USA
E-mail: mscheibner@ucmerced.edu

J Sharping
University of California, Merced, School of Natural Sciences, Merced, CA 95344, USA
E-mail: jsharping@ucmerced.edu

DA Singleton
Department of Physics, California State University Fresno, Fresno, CA 93740-8031, USA
E-mail: dougs@mail.fresnostate.edu

ME Tobar
Quantum Technologies and Dark Matter Labs, Department of Physics, University of Western Australia, Crawley, WA 6009, Australia.
E-mail: michael.tobar@uwa.edu.au

Abstract. In this article, we review a new approach to the scalar Aharonov-Bohm effect for both the electromagnetic and gravitational interaction. For both interactions a quantum system is placed in a time-dependent electromagnetic or gravitational potential, but with no force (spatial derivative of the potential) acting on the quantum system. Nevertheless, we show that the energy levels of the quantum system develop side bands which can be detected as the signature of this version of the scalar Aharonov-Bohm effect. We briefly look at the specific experimental setups required to detect the energy side bands.

1. The Time-Dependent Scalar/Electric Aharonov-Bohm effect

Prior to the seminal work by Aharonov and Bohm in reference [1] the standard view was that it was only derivatives of the potential of a particular interaction (*i.e.* the force associated with the interaction) that led to physical results, while the potentials of the interaction were a mathematical convenience. However, Aharonov and Bohm in [1] showed that the potentials associated with a given interaction had more physical reality than had previously been thought.

The best-known version of the Aharonov-Bohm (AB) effect involves the vector potential (*i.e.* $\mathbf{A}$) and magnetic field (*i.e.* $\mathbf{B} = \nabla \times \mathbf{A}$) of electromagnetism. In the idealized version of this vector/magnetic AB effect, an infinite solenoid is placed between the slits of a double-slit experiment for some quantum particle – normally electrons. The signature of this vector/magnetic AB effect is a shift of the interference pattern that depends on the magnetic flux inside the solenoid. This shift occurs despite the electrons moving entirely in a magnetic field-free region. This vector/magnetic version of the AB effect was first confirmed experimentally by Chambers [2]. A loophole-free version of the vector/magnetic AB effect using a micro-scale torus rather than an infinite solenoid was carried out in an experiment by Tonomura *et al.* [3].

There is also a scalar/electric version of the AB effect which involves the scalar potential (*i.e.* ϕ_e) and electric field (*i.e.* $\mathbf{E} = -\nabla\phi_e$). In this proceeding we focus on the scalar interaction $e\phi_e$ – the product of electric charge, e, with scalar potential, ϕ_e. *i.e.* the scalar coupling between the charge and the electric scalar potential. The original set-up for the scalar/electric AB effect is shown in Fig. 1, where a path of a charged particle is split and sent through two different, spatially separated metal tubes (Faraday cages), which are kept at different potentials while the charged particle is inside the tubes, but with the potential difference (and electric field) turned off when the charged particle is outside the tubes. When the paths of the charged particle are recombined they show a phase difference proportional to the product of the size of the potential difference and the time in the tubes. This version of the scalar/electric AB effect is harder to realize in practice due to the need to synchronize the turning off and on of the potential difference with the charged particle exiting and entering the tube. Because of this, the experimental verification of the scalar/electric AB effect is much less robust than the vector/magnetic AB effect. A well-known experimental verification of the scalar/electric AB effect was given in [4]. However, this experiment measured the effects of both the scalar electric and vector AB effect, rather than the effect of only the scalar electric AB effect. Also at some point in the experiment, the electrons did move in a region where the **E**-field was non-zero. Thus this was not a clean/pure test of the scalar/electric AB effect.

In [5] we proposed a new and cleaner version of the scalar/electric AB effect. The experimental set-up for our proposal to test the scalar electric AB effect, as given in Fig. 2, consists of a Faraday shell of radius R with a time-varying voltage. Outside R there is a time-varying $\mathbf{E}(t)$ field and time-varying scalar potential $\phi_e(t)$, while inside R there is only a time-varying potential, $\phi_e(t)$. The **E** field inside is zero. Next, we place a quantum system (*i.e.* a hydrogen-like atom like rubidium) inside this Faraday shell. In the next section we will show that this leads to the generation of additional energy levels - *i.e.* side-bands - in the quantum system. It is these energy side-bands that are the signature of this version of the scalar/electric AB effect.

It is useful to compare and contrast the two different approaches - from Fig. 1 versus Fig. 2 - to the scalar/electric AB effect. In the original set-up in Fig. 1, charged particles are spatially separated and then recombined after the potential difference has been turned on while the charges are inside the Faraday tubes, and then off when they are outside the tubes. The signature of this version of the scalar/electric AB effect is a phase difference between the two paths that the charged particles took. In the new set-up in Fig. 2, the quantum system is in one spatial location and the potential is varied with time. This exposes the quantum system to a time-varying potential but zero **E**-field. The signature of the setup in Fig. 2 is a shifting of energy levels (or more precisely the generation of energy side bands) rather than a shifting of

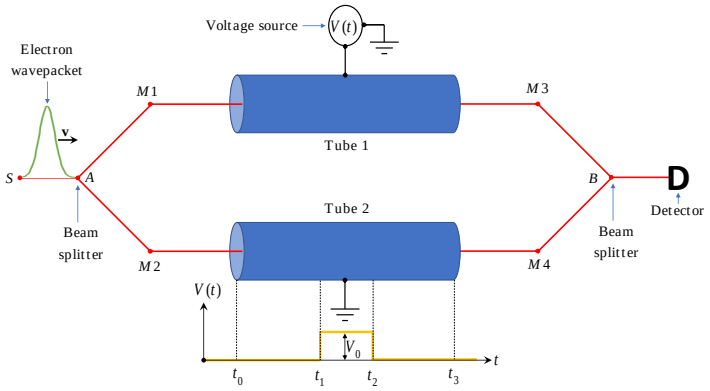

Figure 1. The originally proposed setup for the electric AB effect.

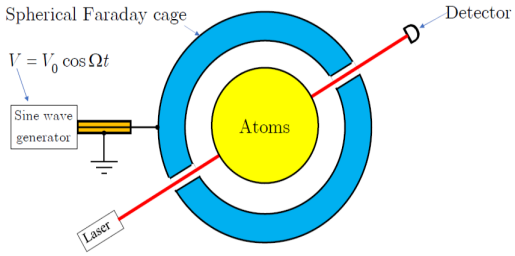

Figure 2. The basic set-up of our proposed test of the scalar electric AB effect

interference fringes. This shifting of the energy levels for the set-up in Fig. 2 is similar to what happens in the ac Stark effect [6, 7] and later we show that the mathematical analysis of the scalar/electric AB effect in Fig. 2 is almost identical to the analysis of the ac Stark effect.

2. General analysis of scalar AB effect

Here we give a general analysis for a quantum system that sees a time-varying, but spatially uniform potential. Since the potential is spatially uniform the force field associated with this potential will be zero since the force field is proportional to the spatial derivative of the potential. Thus the quantum system will see a time-varying potential but a zero force field.

To start we assume that our quantum system is described by a Hamiltonian, H_0, for which the solutions to the time-independent Schrödinger equation are known *i.e.* $H_0\Psi_i(\mathbf{x}) = E_i\Psi_i(\mathbf{x})$. We now place this quantum system in a time-varying, spatially uniform potential, $V(t)$, with a "charge" Q so that the total Hamiltonian is

$$H = H_0 + QV(t) \tag{1}$$

In section 3 we will take $V(t)$ to be the electric scalar potential, ϕ_e, and the "charge" to be the electric charge, $Q = e$, while in section 4 we will take $V(t)$ to be the gravitational scalar potential, ϕ_g, and the "charge" to be mass, $Q = m$. We take $V(t)$ to be sinusoidal of the form

$$\begin{aligned} V(t) &= 0 \quad \text{for } t < 0 \\ V(t) &= V_0 \cos\Omega t \quad \text{for } t \geq 0\ . \end{aligned} \tag{2}$$

$\frac{\Omega}{2\pi}$ is the frequency and V_0 is the amplitude. For $t < 0$ where $V(t) = 0$ the Hamiltonian is just H_0 with wave function solutions $\Psi_i(\mathbf{x})$, and energy eigenvalues E_i. The time-dependent Schrödinger equation for this new system is

$$i\hbar\frac{\partial\psi}{\partial t} = H\psi = (H_0 + QV(t))\,\psi \tag{3}$$

Hamiltonians of the form (3) with a piecewise, continuous periodic potential can be solved using Floquet's theorem. We briefly run through the solution of (3).

We begin by applying the separation-of-variables ansatz $\psi(\mathbf{x}, t) = X(\mathbf{x})T(t)$. Substituting this into (3) gives

$$i\hbar\frac{\partial\psi}{\partial t} = i\hbar X\frac{dT}{dt} = (H_0 + QV)\,XT = TH_0X + X\,(QV)\,T \tag{4}$$

Dividing by XT and moving the $QV(t)$ term to the left-hand side gives

$$-QV + i\hbar\frac{1}{T}\frac{dT}{dt} = \frac{1}{X}H_0X \tag{5}$$

Since the left-hand side of this equation only depends on t while the right-hand side only depends on $\mathbf{x}$ each side must be equal to a constant which we denote as E. This leads to the separated equations

$$-QV + i\hbar\frac{d\ln T}{dt} = E \quad \textit{and} \quad H_0X = EX \tag{6}$$

The solution to the second equation in (6) is just the known solution to the time-independent Schrödinger equation namely $X = \Psi_i(\mathbf{x})$ and $E = E_i$ *i.e.* $H_0\Psi_i(\mathbf{x}) = E_i\Psi_i(\mathbf{x})$. Next we integrate the first, temporal equation in (6) over t giving

$$-Q\int V(t)dt + i\hbar\int\frac{d\ln T(t)}{dt}dt = \int E_i dt \tag{7}$$

Carrying out the integrations in (7) and solving for $T(t)$, gives

$$\begin{aligned} T(t) &= \exp\left(-\frac{i}{\hbar}E_it\right)\exp\left(-\frac{i}{\hbar}Q\int V\,dt\right) \\ &= \exp\left(-\frac{i}{\hbar}E_it - i\alpha\sin\Omega t\right) = \exp\left(-\frac{i}{\hbar}E_it - i\varphi(t)\right)\ , \end{aligned} \tag{8}$$

where α is called the FM depth of modulation parameter and is defined as

$$\alpha = \frac{QV_0}{\hbar\Omega} \tag{9}$$

Multiplying $X(\mathbf{x}) = \Psi_i(\mathbf{x})$ and $T(t)$ from (8) gives the wave function, $\psi_i(\mathbf{r}, t)$, for the full Hamiltonian, $H_0 + QV(t)$ from (1) gives

$$\psi_i(\mathbf{r}, t) = \Psi_i(\mathbf{r})\exp\left(-\frac{iE_it}{\hbar} - i\varphi(t)\right)\ . \tag{10}$$

This new wave function is the original wave function with an added AB phase factor $\exp(-i\varphi(t))$. From (8) the AB phase, $\varphi(t)$, is given by

$$\varphi(t) = \frac{Q}{\hbar}\int V(t)dt = \alpha\sin\Omega t\ . \tag{11}$$

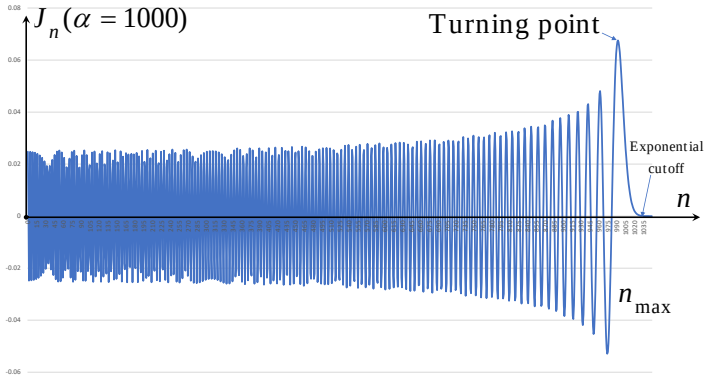

Figure 3. A plot of $J_n(\alpha)$ vs. n for the case when $\alpha = 1000$. There are side-bands in the energy $E_i^{(n)}$ which occurs up to some maximum index n given by $n_{max} \approx \alpha$. From the plot, one can see that the weighting, $J_n(\alpha)$, is largest when $n = n_{max} \approx \alpha$ and it is this state which contributes the most.

To see the emergence of the energy side-bands we exponentiate the AB phase from (11) and use the Jacobi-Anger expansion [1]

$$\exp\left(-i\varphi(t)\right) = \exp\left(-i\alpha\sin\Omega t\right) = \sum_{n=-\infty}^{\infty}(-1)^n J_n(\alpha)\exp\left(in\Omega t\right) \ . \tag{12}$$

Using (12) in (10), the wave function now reads

$$\begin{aligned}\psi_i(\mathbf{r},t) &= \Psi_i(\mathbf{r})\sum_{n=-\infty}^{\infty}(-1)^n J_n(\alpha)\exp\left(in\Omega t\right)\exp\left(-\frac{iE_i t}{\hbar}\right) \\ &= \Psi_i(\mathbf{r})\sum_{n=-\infty}^{\infty}(-1)^n J_n(\alpha)\exp\left(-\frac{i\left(E_i - n\hbar\Omega\right)t}{\hbar}\right)\end{aligned} \tag{13}$$

Reading off (13) we can see that each energy level E_i is split into a series of energy side-bands, $E_i^{(n)}$, given by

$$E_i^{(n)} = E_i \pm n\hbar\Omega, \text{ with } n, \text{an integer} \tag{14}$$

Equation (14) would seem to imply that there is an infinite ladder of energy levels above and below E_i characterized by integer multiples of $\hbar\Omega$. However, this ignores the Bessel function "weighting" factor $J_n(\alpha)$ for each oscillator term from (13). If one plots this weighting factor as a function of n (see Fig. 3) one sees that beyond a maximum value of n the contributions to $\psi_i(\mathbf{r},t)$ are exponentially suppressed. From Fig. 3 one can see that this maximum value of n is approximately equal to the value of α *i.e.*

$$n_{max} \approx \alpha \ . \tag{15}$$

Effectively one only has a finite number of energy side bands that run up to $n = n_{max} \approx \alpha$. Further from Fig. 3 one sees that the maximum weighting, $J_n(\alpha)$, occurs also at this n_{max} so

[1] The Jacobi-Anger expansion replaces the exponential of a sinusoidal function with an infinite series of the product of Bessel function $J_n(\alpha)$ and oscillatory functions of the form $\exp\left(in\Omega t\right)$.

that one can approximate the energy side-bands as consisting only of one upper and one lower side-band

$$E_i \pm n_{max}\hbar\Omega \approx E_i \pm QV_0 \ , \tag{16}$$

where in the last step in (16) we have used $n_{max} \approx \alpha = \frac{QV_0}{\hbar\Omega}$.

In conclusion, the generic scalar AB phase, $\varphi(t)$, creates energy side bands, equations (14) (16), which can be probed for via spectroscopic experiments. The dominant energy side-bands occur for $n = n_{max} \approx \alpha$. These energy side-bands are essentially the quasi-energy levels of Zeldovich [8] and studied later in more detail by Sambe [9].

3. Electric scalar AB effect

To apply the above results of section 2 to the electric/scalar AB effect we simply need to take $Q \to e$ (general charge goes to electric charge) and $V(t) \to \phi_e$ (general potential goes to electric scalar potential). With these changes, the results of section 2 can be used for our version of the scalar/electric AB effect as sketched in Fig. 2.

In reference [5] it was shown that our version of the scalar/electric AB effect from Fig. 2 was mathematically similar to the ac Stark effect (also known as the Autler-Townes effect) [6]) which also led to the generation of energy side bands as in (16). Physically the ac Stark effect is different from our set-up in Fig. 2 since in the ac Stark effect the quantum system sees a non-zero vector potential and non-zero electric field, while in the scalar/electric AB set-up from Fig. 2 the quantum system sees only a time-varying scalar potential.

The difference between the ac Stark effect and our version of the scalar/electric AB effect can be seen in how the vector and scalar potentials are coupled to the charge e. Starting from the time-independent Schrödinger equation, $i\hbar\frac{\partial}{\partial t}\Psi = \frac{\hat{\mathbf{p}}^2}{2m}\Psi$ for a particle of mass m and charge e, for the ac Stark effect, one uses minimal coupling of the vector potential $\hat{\mathbf{p}}^2 \to (\hat{\mathbf{p}} - e\mathbf{A})^2$. The vector potential in this case is taken as $\mathbf{A}(t) = \frac{E_0}{\Omega}\cos(\Omega t)\hat{\mathbf{z}}$, which leads to an electric field of $\mathbf{E} = -\frac{\partial \mathbf{A}}{\partial t} = E_0 \sin(\Omega t)\hat{\mathbf{z}}$. Following the analysis of the ac Stark effect from [7] shows that the quantum system will develop energy side-bands of the form given in (16). For the scalar/electric AB effect, the minimal coupling of the scalar potential is accomplished via $i\hbar\frac{\partial}{\partial t} \to i\hbar\frac{\partial}{\partial t} - e\phi_e(t)$ with $\phi_e(t) = V_0\cos(\Omega t)$. Then via the analysis in section 2 one also sees side-bands of the form given in (16). Now however, the quantum system sees only the scalar potential; the electric field is zero since $\mathbf{E} = -\nabla\phi_e(t) = 0$. The ac Stark effect has been observed experimentally, and we proposed in [5] that one should be able to observe the scalar/electric AB effect as similarly given in Fig. 2.

As a final comment on this version of the scalar/electric AB effect one can question this setup in Fig. 2 (and detailed in section 2) since it is possible to gauge away the scalar potential, $\phi_e(t) = V_0\cos(\Omega t)$. A general gauge transformation of the scalar and vector potential is

$$\phi_e' = \phi_e - \partial_t\lambda \quad \text{and} \quad \mathbf{A}' = \mathbf{A} + \nabla\lambda \ , \tag{17}$$

with the gauge function $\lambda(\mathbf{r}, t)$. By choosing $\lambda(t) = \frac{V_0}{\Omega}\sin(\Omega t)$ one can cancel out $\phi_e(t) = V_0\cos(\Omega t)$ so that $\phi_e' = 0$. Also since $\nabla\lambda = 0$ the new vector potential will remain zero, $\mathbf{A}' = 0$. Thus one has gauge transformed away all electromagnetic potentials so how can there be any effect? The resolution to this question is that (17) is only half of the gauge transformation. One must also transform the wave function as

$$\begin{aligned} \psi_i'(\mathbf{r}, t) &= \exp\left(-i\frac{e}{\hbar}\lambda\right)\psi_i(\mathbf{r}, t) = \exp\left(-i\frac{eV_0}{\hbar\Omega}\sin(\Omega t)\right)\Psi_i(\mathbf{r})\exp\left(-i\frac{E_i t}{\hbar}\right) \\ &= \Psi_i(\mathbf{r})\exp\left(-i\frac{E_i t}{\hbar} - i\varphi(t)\right) \ . \end{aligned} \tag{18}$$

In arriving at the results in (18) we have used results from (10) and (11). The wave function ψ' from (18), which is in the gauge where all electromagnetic potentials are zero, matches the wave function ψ from (10) which has the non-zero, sinusoidal scalar potential. The results leading to the energy side bands are gauge invariant.

4. Gravitational AB effect

In this section, we show that one can set up a gravitational version of the scalar/electric AB effect discussed above in sections 2 and 3. The gravitational AB phase can be obtained from the general formula in (11) by letting $Q \to m$ (generic charge goes to mass) and $V(t) \to \phi_g(t)$ (generic potential goes to gravitational potential. This gives the gravitational AB phase as

$$\varphi_g(t) = \frac{m}{\hbar}\int_0^t \phi_g(t')dt' \ . \tag{19}$$

For the scalar/electric AB effect, the quantum system was placed inside a Faraday cage with a sinusoidal varying potential, $\phi_e(t) = V_0\cos(\Omega t)$ - see Fig. 2. This does not work for the gravitational case, for reasons discussed below and in more detail in [10]. For the gravitational AB effect, we will instead place our quantum system in a satellite in an elliptical orbit so that the distance between the satellite and center of the Earth changes with time. Thus the gravitational potential will be of the form

$$\phi_g(t) = -\frac{GM}{r(t)} \tag{20}$$

where G is Newton's constant, M is the mass of some large body (*e.g.* the Earth) about which our quantum system will orbit, and $r(t)$ is the time-dependent distance between the satellite and one focus of the orbit *i.e.* the center of the Earth. In the scalar/electric AB effect set-up we varied the scalar potential, $\phi_e(t)$, by varying the charges oscillated onto and off of the Faraday shell *i.e.* the charge on the shell was time-dependent $e(t)$. A similar set-up for the gravitational interaction would require varying the mass rapidly *i.e.* $M \to M(t)$. This is not practical, and so we vary the radius $r \to r(t)$, by placing the quantum system in an elliptical orbit.

Since our quantum system is in orbit (free fall) in a satellite, then by the equivalence principle the quantum system will be locally in a zero gravitational field, *i.e.* the field has been transformed away by going to a free falling frame.

First we consider the orbit of the International Space Station (ISS), which is an almost circular, low Earth orbit with orbital parameters given by: (i) perigee and apogee radius from the center of the Earth are $r_p = 6.800\times10^6$ m and $r_a = 6.810\times10^6$ m, respectively, which corresponds to a perigee altitude of 400 km and apogee altitude of 410 km given that the Earth's radius is $r_E \approx 6400$ km. (ii) The period of the ISS with this apogee/perigee is about $T \approx 90$ minutes or 5400 seconds giving an angular frequency of $\Omega = \frac{2\pi}{T} = 1.0\times10^{-3}\frac{\text{rad}}{\text{sec}}$ (or a standard frequency of $f = 1.59\times10^{-4}$ Hz). The radius of the orbit as a function of time can be approximated as [2]

$$r(t) = \frac{r_p + r_a}{2} + \frac{r_p - r_a}{2}\cos(\Omega t) \equiv A + B\cos(\Omega t) \ . \tag{21}$$

Using the r_p and r_a values above, we find the A and B parameters defined in (21) become $A = 6.805\times10^6$ m and $B = -5.000\times10^3$ m. Perigee occurs at $t = 0$ and apogee at $t = \pi/\Omega$. For the chosen r_a and r_p, $A \gg B$ so one can approximate $\frac{1}{r(t)} = \frac{1}{A+B\cos(\Omega t)} \approx \frac{1}{A}\left(1 - \frac{B}{A}\cos(\Omega t)\right)$. With this the gravitational potential in (20) becomes

$$\phi_g(t) \approx -\frac{GM}{A}\left[1 - \frac{B}{A}\cos(\Omega t)\right] \ , \tag{22}$$

[2] This treatment of nearly circular orbits is essentially that found in section 9.5 of reference [11]

Inserting this in (19) gives

$$\varphi_g(t) = -\frac{GmM}{\hbar A}\int_0^t \left(1 - \frac{B}{A}\cos(\Omega t')\right) dt' \ . \tag{23}$$

The second sinusoidal term in (23) gives the gravitational AB phase. The term linear in t is packaged with the energy to give a shift of the base energy of the quantum system.

With (22) and (23) in hand we can repeat the analysis in section 2 (from (1) through (16)) to obtain the result for the gravitational AB effect.

As before, in the absence of the gravitational potential, $\phi_g(t)$, we assume that the quantum system has a known solution to the time-independent Schrödinger (*i.e.* $H_0\Psi_i(\mathbf{x}) = E_i\Psi_i(\mathbf{x})$) where H_0, Ψ_i and E_i are the Hamiltonian, wavefunction and energy eigenvalues, respectively, of the quantum system. Placing the quantum system in the potential, $\phi_g(t)$, leads to the Hamiltonian $H = H_0 + m\phi_g(t)$, with the new term being the time-dependent gravitational potential energy. The Schrödinger equation for H is analogous to (3)

$$i\hbar\frac{\partial\psi}{\partial t} = H\psi = \left(H_0 + m\phi_g(t)\right)\psi. \tag{24}$$

At this point we solve (24) exactly using separation-of-variables with $\psi(\mathbf{x},t) = X(\mathbf{x})T(t)$. As before the spatial part of this solution is just $X = \Psi_i(\mathbf{x})$ and the energy eigenvalue is $E = E_i$. These are the given solutions to the time-independent Schrödinger equation $H_0\Psi_i(\mathbf{x}) = E_i\Psi_i(\mathbf{x})$.

Carrying out steps similar to those in section 2 we find that the time part of the separation of variables is

$$\begin{aligned} T(t) &= \exp\left(-\frac{i}{\hbar}E_i t\right)\exp\left(-\frac{i}{\hbar}m\int\phi_g dt\right) \\ &= \exp\left(-\frac{i}{\hbar}\left(E_i + \frac{GmM}{A}\right)t - i\alpha\sin\Omega t\right) \\ &= \exp\left(-\frac{i}{\hbar}\left(E_i + \frac{GmM}{A}\right)t - i\varphi_g(t)\right) \ , \end{aligned} \tag{25}$$

where $\alpha \equiv \frac{GmMB}{\hbar\Omega A^2}$ is the dimensionless gravitational depth of modulation parameter. To obtain a value for α we assume the satellite orbits the Earth so that $M = 5.97\times10^{24}$ kg. The value of A and B for the almost circular orbit are given above (22) as $A = 6.805\times10^6$ m and $B = -5.000\times10^3$ m, and the angular frequency given above (21) is $\Omega = \frac{2\pi}{T} = 1.0\times10^{-3}\frac{\text{rad}}{\text{sec}}$. If the quantum system is an atomic system, $m \to m_e = 9.11\times10^{-31}$ kg (the electron mass), and if it is a nuclear system $m \to m_N = 1.67\times10^{-27}$ kg (the nucleon mass). If the system for comparison is a photon, which is absorbed by a quantum system, then the energy level is the difference between two quantum states with a rest mass increase of $m_{ph} = E_{ph}/c^2$. Using these values for A, B, M, Ω and m we find $\alpha_{atomic} \approx -3.7\times10^{11}$ for atomic systems, $\alpha_{nuclear} \approx -6.8\times10^{14}$ for a nuclear system and $\alpha_{ph} \approx -2.6 f_{ph}$ for the photonic system, where f_{ph} is the photon frequency in GHz.

The $\frac{GmM}{A}$ term in (25) gives a constant shift to the unperturbed energy E_i which was not present in the scalar/electric AB effect. In the scalar/electric AB case, this constant part of the electric potential was equal to zero. It is only the $\varphi_g(t)$ term in (25) which is associated with the gravitational AB effect.

Combining the spatial part of the solution $X(\mathbf{x}) = \Psi_i(\mathbf{x})$ and the temporal part of the solution $T(t)$ from (8) gives the wave function, $\psi_i(\mathbf{r},t)$ as

$$\psi_i(\mathbf{r},t) = \Psi_i(\mathbf{r})\exp\left(-\frac{i\left(E_i + \frac{GmM}{A}\right)t}{\hbar} - i\varphi_g(t)\right) \ . \tag{26}$$

This new wave function is the original wave function with an added AB phase factor $\exp(-i\varphi_g(t))$, with the gravitational AB phase given by $\varphi_g(t) = \frac{m}{\hbar}\int \frac{GMB}{A^2}\cos(\Omega t)dt = \alpha \sin\Omega t$. Again using the Jacobi-Anger expansion to evaluate the exponentiation of $\varphi_g(t)$ gives the wave function as

$$\begin{aligned}\psi_i(\mathbf{r},t) &= \Psi_i(\mathbf{r})\sum_{n=-\infty}^{\infty}(-1)^n J_n(\alpha)\exp(in\Omega t)\exp\left(-\frac{i\left(E_i+\frac{GmM}{A}\right)t}{\hbar}\right)\\ &= \Psi_i(\mathbf{r})\sum_{n=-\infty}^{\infty}(-1)^n J_n(\alpha)\exp\left(-\frac{i\left(E_i+\frac{GmM}{A}-n\hbar\Omega\right)t}{\hbar}\right)\end{aligned} \tag{27}$$

The result in (27) is similar to the generic AB analysis in (13) and we can see that each energy level E_i is split into a multiplet $E_i^{(n)}$

$$E_i^{(n)} = E_i + \frac{GmM}{A} \pm n\hbar\Omega \equiv \tilde{E}_i \pm n\hbar\Omega, \quad \text{with } n, \text{an integer .} \tag{28}$$

In distinction from the generic result of (14) the result in (28) has a constant shift of $\frac{GmM}{A}$ which we have absorbed into the definition of $\tilde{E}_i$. It is the energy side bands represented by $\pm n\hbar\Omega$ which are signature for this version of the AB effect. Note, if we consider comparing photons from stable clocks in different potentials then $\tilde{E}_i = E_i(1+\frac{GM}{c^2A})$, which is equivalent to the energy/frequency shift of the photon due to the gravitational potential, which causes the gravitational redshift of a photon as it escapes a gravitational potential.

5. Experimental set-up and considerations

In this short section, we summarize and briefly discuss some of the details and issues associated with this new proposal to probe both the scalar/electric AB effect and the gravitational AB effect.

5.1. Experimental set-up for scalar/electric AB effect

The new version of the scalar electric AB effect, shown in Fig. 2, is cleaner than the original proposal shown in Fig. 1. We do not have to time the turn-on and turn-off of the potential difference with the charge entering or exiting the metal tubes. Also for the setup in Fig. 1, there are always fringing fields, while for the Faraday sphere setup, the electric field is zero inside the shell, modulo very small electric and magnetic fields that arise whenever there is a time variation in charges/fields.

A full discussion of the experimental details to probe this version of the scalar/electric AB effect can be found in [5]. In order to ensure that only the side bands with $n = n_{max} \approx \alpha = \frac{eV_0}{\hbar\Omega}$ dominate one needs to have $QV_0 \to eV_0 \gg \hbar\Omega$ or $\alpha \gg 1$. In [5] it was shown that this condition was easy to achieve for obtainable values of V_0 and Ω (in [5] we chose $V_0 = 0.5mV$, and $\Omega = 10^8$ s^{-1} which gave $\alpha \approx 10^4$).

Another avenue to probe the energy sidebands of (16) was to use electromagnetically induced transparency (EIT). Details of this can be found in [5].

5.2. Experimental set-up for gravitational AB effect

We briefly review some details of the experimental setups to probe the gravitational AB effect. From equation (28) it again seems that there are an infinite number of energy sidebands above and below $\tilde{E}_i$. However, using Fig. 2 and as discussed below (16) it is only the two energy side bands with $n = n_{max} \approx \alpha$ which will dominate if the condition $\alpha \gg 1$ is met. For the

ISS orbit this will be true for atomic and nuclear system, but only for the photonic system if $f_{ph} \gg 340MHz$.

In contrast to the scalar/electric AB effect, which only has one unit of charge ($Q = e$), the gravitational AB effect has several possible charges depending on the mass of the particle of the quantum state. If the quantum system in the satellite is atomic (in this case $Q = m_e$ with m_e being the electron mass) or nuclear (in this case $Q = m_N$ with m_N being the nucleon mass.) Using the numerical values for $A, B, \Omega, M, m_e, m_N$ below (25) gives $|\alpha_{atomic}| \approx 3.7\times10^{11} \approx n_{max}$, and for atomic systems, $|\alpha_{nuclear}| \approx 6.8\times10^{14} \approx n_{max}$ for nuclear systems. For a photonic system generated by a nuclear or atomic transition, the change in rest mass, m_{ph}, of the particle in the excited state depends on the energy of the transition through $E_{ph} = m_{ph}c^2 = hf_{ph}$, and for the ISS orbit $|\alpha_{ph}| \approx 2.9 \times 10^{-9} f_{ph}$, where f_{ph} is in Hz.

The issue becomes if one can observe the energy side bands given their magnitude. In [10] it was shown that one could observe the energy sidebands using the ACES (Atomic Clock Ensemble in Space) mission [12], which involves putting optical/microwave frequency clocks on the ISS. For the nuclear case reference [10] proposed using the Mössbauer effect to observe the energy sidebands. This was a temporal version of the famous Pound-Rebka experiment [14]. The Pound-Rebka experiment observed the gravitational shift of gamma rays emitted and absorbed by ^{57}Fe with the emitter and absorber being spatially separated vertically in a gravitational field. Here the emission and absorption are temporally separated due to the change of the satellite as it orbits the Earth. More experimental details about both the atomic and nuclear probes for the gravitational AB effect are in reference [10].

Data from Galileo satellites in eccentric orbits, which have been used to put the best limits on the redshift from the comparison of onboard hydrogen maser clocks with ground clocks [15, 16], may also be used to search for effects of the gravitational AB effect. When a photon excites an energy transition and is absorbed, the mass of the excited electron increases through a quantum electrodynamics virtual process, given by $\Delta m_e = \frac{hf_{ph}}{c^2}$. Thus, these eccentric orbits, which will experience a significant modulation of the gravitational potential, will in turn cause the energy levels of the hydrogen maser transition to change and hence the mass of the excited hydrogen atoms to vary. In this case the DC term in (28) is equivalent to the redshift, which was measured in [15, 16] at a precision of parts in 10^5, while the Aharonov-Bohm phase proposed here predicts extra sidebands. The orbital period of these Galileo satellite is 12.94 hours (21.5 μHz) with an eccentricity of $e = 0.162$, with a perigee and apogee radius from the center of the Earth of $r_p = 23,445km$ and $r_a = 32,510km$, respectively, so $A_G = 27,977.5$ km, and $B_G = -453.2$ km and thus the gravitational modulation parameter for the Galileo orbit, given by (9), is $\alpha_G \equiv \frac{G\Delta m_e M B_g}{\hbar\Omega A_g^2} = 1.2 \times 10^{-6} f_{ph}$ where f_{ph} is in Hz. For the hydrogen maser clock transition at 1.42 GHz, $\alpha_G = 1699$, with a predicted maximum modulation sideband at around 26.2 mHz. Note, that this orbit causes a depth in modulation, α_G, which is more than 450 times greater than the modulation index induced by the ISS orbit, which the ACES clocks experience.

5.3. Acknowledgments

MET was funded by the ARC Centre of Excellence for Engineered Quantum Systems, CE170100009, and Dark Matter Particle Physics, CE200100008

References

[1] Y. Aharonov and D. Bohm, Phys. Rev. **115**, 485 (1959).
[2] R.G. Chambers, Phys. Rev. Lett. **5**, 3 (1960).
[3] A. Tonomura *et al.*, Phys. Rev. Lett. **56**, 792 (1986).
[4] A. van Oudenaarden, M.H. Devoret, V. Yu. Nazarov, and J.E. Mooij, *Nature*, **391**, 768 (1998)
[5] R. Chiao, H. Hart, M. Scheibner, J. Sharping, N. Inan, D. Singleton, and M. Tobar Phys. Rev. A **107**, 042209 (2023).

[6] S.H. Autler and C. H. Townes, Phys. Rev., **100**, 703 (1955).
[7] N.B. Delone and V.P. Krainov, Physics-Uspekhi, **42**, 669 (1999).
[8] Y. Zel'dovich, Sov. Phys.-JETP **24**, 1006 (1967).
[9] H. Sambe, Phys. Rev. A **7**, 2203 (1973).
[10] R. Chiao, N. Inan, M. Scheibner, J. Sharping, D. Singleton, and M. Tobar, "Gravitational Aharonov-Bohm Effect", e-Print: 2311.07764 [gr-qc].
[11] D. Kleppner and R.J. Kolenkow, *An Introduction to Mechanics*, (McGraw Hill, Boston, MA 1973).
[12] L. Cacciapuoti, *et al.*, Eur. Phys. J. D, **74**, 164 (2020).
[13] R.L. Mössbauer, Zeit. Phys. A, **151**, 124 (1958).
[14] R.V. Pound and G.A. Rebka, Phys. Rev. Letts. **4**, 337 (1960).
[15] Sven Herrmann, Felix Finke, Martin Lülf, Olga Kichakova, Dirk Puetzfeld, Daniela Knickmann, Meike List, Benny Rievers, Gabriele Giorgi, Christoph Günther, Hansjörg Dittus, Roberto Prieto-Cerdeira, Florian Dilssner, Francisco Gonzalez, Erik Schönemann, Javier Ventura-Traveset, and Claus Lämmerzahl, eccentric orbit," *Phys. Rev. Lett.*, vol. 121, pp. 231102, Dec 2018.
[16] P. Delva, N. Puchades, E. Schönemann, F. Dilssner, C. Courde, S. Bertone, F. Gonzalez, A. Hees, Ch. Le Poncin-Lafitte, F. Meynadier, R. Prieto-Cerdeira, B. Sohet, J. Ventura-Traveset, and P. Wolf, *Phys. Rev. Lett.*, vol. 121, pp. 231101, Dec 2018.